HOKKAIDO UNIVERSITY

Title	Insights into Geometries, Stabilities, Electronic Structures, Reactivity Descriptors, and Magnetic Properties of Bimetallic NimCun-m (m=1, 2; n=3-13) Clusters: Comparison with Pure Copper Clusters
Author(s)	Singh, Raman K.; Iwasa, Takeshi; Taketsugu, Tetsuya
Citation	Journal of computational chemistry, 39(23), 1878-1889 https://doi.org/10.1002/jcc.25361
Issue Date	2018-09-05
Doc URL	https://hdl.handle.net/2115/75435
Rights	This is the peer reviewed version of the following article: Journal of Computational Chemistry, Volume39, Issue23, September 5, 2018, Pages 1878-1889, which has been published in final form at https://doi.org/10.1002/jcc.25361 . This article may be used for non-commercial purposes in accordance with Wiley Terms and Conditions for Use of Self-Archived Versions.
Type	journal article
File Information	NiCu-JCC-hokudai.pdf

Hokkaido University Collection of Scholarly and Academic Papers : HUSCAP

Insights into Geometries, Stabilities, Electronic Structures, Reactivity Descriptors, and Magnetic Properties of Bimetallic Ni_mCu_{n-m} (m = 1, 2; n = 3-13) Clusters: Comparison with Pure Copper Clusters

Raman K. Singh,[a,b] *Takeshi Iwasa*,[a,c] and *Tetsuya Taketsugu**[a,c]

---

[a] *Raman K. Singh*, *Takeshi Iwasa*, *Tetsuya Taketsugu*

Elements Strategy Initiative for Catalysts and Batteries (ESICB), Kyoto University, Kyoto 615-8245, Japan

[b] *Raman K. Singh*

Department of Chemistry, Jagdam College, Chapra Jai Prakash University, Chapra, Bihar - 841301, India

[c] *Takeshi Iwasa, Tetsuya Taketsugu*

Department of Chemistry, Faculty of Science, Hokkaido University, Sapporo 060-0810, Japan

Corresponding author (Tetsuya Taketsugu)

E-mail: take@sci.hokudai.ac.jp

ABSTRACT:

A long-range corrected density functional theory (LC-DFT) was applied to study the geometric structures, relative stabilities, electronic structures, reactivity descriptors and magnetic properties of the bimetallic $NiCu_{n-1}$ and Ni_2Cu_{n-2} (n = 3-13) clusters, obtained by doping one or two Ni atoms to the lowest energy structures of Cu_n, followed by geometry optimizations. The optimized geometries revealed that the lowest energy structures of the $NiCu_{n-1}$ and Ni_2Cu_{n-2} clusters favor the Ni atom(s) situated at the most highly coordinated position of the host copper clusters. The averaged binding energy, the fragmentation energies and the second-order energy differences signified that the Ni doped clusters can continue to gain an energy during the growth process. The electronic structures revealed that the highest occupied molecular orbital (HOMO) and the lowest unoccupied molecular orbital (LUMO) energies of the LC-DFT are reliable and can be used to predict the vertical ionization potential and the vertical electron affinity of the systems. The reactivity descriptors such as the chemical potential, chemical hardness and electrophilic power, and the reactivity principle such as the minimum polarizability principle are operative for characterizing and rationalizing the electronic structures of these clusters. Moreover, doping of Ni atoms into the copper clusters carry most of the total spin magnetic moment.

Introduction

During the last few decades, transition-metal clusters have attracted much attention because of their physical and chemical properties that are different from those of bulk metals. The typical advantage of the clusters involves catalytic activities, stability and easy recovery. Since the clusters have the large surface-to-volume ratio leading to the unique geometries, electronic and magnetic properties, a detailed study of the evolution of the structural, relative stabilities, electronic and magnetic properties of the clusters is always indispensable to bridge our understanding over atoms, nanoparticles and the bulk.[1,2]

Nowadays there is a growing demand on nonprecious-metal catalysts due to a limited amount of precious metals, and the catalytic activity of copper nanoclusters has emerged as one of the promising candidates in various areas of sensing,[3,4] biolabeling,[5] and catalysis.[6–14] This is apparent reason that copper clusters are currently the hot topics in research. However, the controlled synthesis, stabilization and characterization of small clusters is a cumbersome task,[15,16] and quantum chemical studies provide the geometric, electronic, and chemical properties to understand the origin of the exceptional catalytic activity. To this end, the reactivity of copper clusters, and its evaluation with the number of atoms in the cluster, has been investigated theoretically[17–26] but much more need still to be done to design a better catalyst.

In 1960s, the concept of bimetal was proposed, and since then bimetallic alloys have been receiving much interests due to their wide range of applications in heterogeneous catalysis. The addition of a second metal to the host metal surface can sometimes dramatically improve the selectivity, activity, and stability in surface-catalyzed reactions.[15,16] Similarly, in cluster chemistry, cluster size, shape, composition and oxidation state are important parameters responsible for affecting the metal cluster properties.[27–31] These properties may dramatically change when doped with another metal atom. The previous studies have shown that bimetallic

nanoalloys are better catalyst than pure metals and they are in demand in various commercial electrocatalytic and catalytic processes.[32,33] Therefore, researchers envisioned that copper clusters doped with different transition-metal atoms will be a new kind of molecular architecture to provide the desired structural, electronic, magnetic, optical and catalytic properties for potential applications in nanotechnology, materials science, microelectronics, biology, medicine and solid-state chemistry.[3–16,34]

Recently, Ni-doped copper alloys have been investigated to exploit their untapped potential for better catalytic performance. For instance, Nerlov et al.[35–37] reported that the Cu-Ni catalysts are 60 times more active for CO_2 activation compared with the pure copper, while Liu et al.[38] found that Pd, Rh, Pt, and Ni metals are able to promote the methanol production on Cu(111). Yang et al.[39] noted that the Cu_{29} nanoparticles with or without ZnO support exhibit a higher catalytic activity than Cu(111) for the methanol synthesis via CO_2 hydrogenation. It indicates that doping of Ni atoms into Cu clusters would be more promising for the catalytic hydrogenation of CO_2 into methanol than the pure copper ones. Moreover, Cheng and his co-workers[39] theoretically studied the role of composition and geometric relaxation in CO_2 binding to the Cu-Ni ($Cu_{54}Ni$, $Cu_{42}Ni_{13}$) bimetallic clusters. It was concluded that icosahedral $Cu_{42}Ni_{13}$ cluster exhibits the strongest CO_2 adsorption ability with respect to Cu_{55} and $Cu_{54}Ni$ clusters. On the other hand, Austin et al.[40] demonstrated that doping of Ni on the surface of CuNi ($Cu_{43}Ni_{12}$, $Cu_{12}Ni_{43}$, $Cu_{42}Ni_{13}$, $Cu_{13}Ni_{42}$) bimetallic nanoparticles can significantly enhance the CO_2 adsorption. Derosa et al.[41] computationally studied a planar configuration of Cu-Ni clusters containing up to five atoms and concluded that Cu clusters with small concentration of Ni could be the best adsorbents for hydrogens. However, Han et al.[42] performed the spin-polarized density functional theory (DFT) calculations using the Projector augmented-wave (PAW) method[43,44] and Perdew-Burke-Ernzerhof (PBE) functional[45] to study the chemical activities of Cu_nNi clusters (n = 1-12) toward the CO_2 adsorption. Since the PAW method was

conceived for solids, its accuracy to deal with molecular systems might be less than that of both DFT and a wave function theory using atom-centered basis functions, and their results may not be directly comparable. In light of above mentioned work, a systematic, in-depth study of the structural evolution and properties of Ni-doped copper clusters are still lacking. This study is, therefore, urgently warranted for designing cheaper and more efficient Ni-Cu catalyst.

Currently, the generalized Kohn-sham (KS) method[46] using the long-range corrected[47] (LC-) DFT has solved many deep-seated problems in conventional DFT methods such as a poor description of van der Waals bonds,[48] an underestimation in excitation energies by time-dependent (TD) DFT,[49,50] poor evaluations of hyperpolarizabilities[51] and valence orbitals energies.[52–54] Despite its huge potential, LC-DFT has not been extensively used for metal-cluster catalysis, to the best of our knowledge. This prompted us to employ such a state-of-the-art DFT functional for both quantitative and qualitative calculations. Therefore, in this work, our purpose is to study Ni-doping effects on geometric, relative stabilities, electronic structures, reactivity descriptors, and magnetic properties for the most stable structure of small copper clusters, Cu_n (n = 3-13), using the long-range corrected DFT. For comparison, the most stable structure of pure copper clusters, Cu_n (n = 3-13), are also systematically studied so that this work could provide practical guidelines for experimental researches in near future.

The paper is organized as follows: in next section 2, a brief description of computational methods is provided. Section 3 is devoted to the results and discussion and in Section 4, we draw our conclusions.

Computational Details

The LC-DFT method, LC-BLYP,[47,55] was employed in conjunction with LANL2DZ basis sets,[56] for computations of all clusters of Ni_mCu_{n-m} (m = 0-2; n = 3-13). The range separation parameter for the LC-BLYP was set 0.47, which is the optimum value for the ground state calculation. To test the reliability of LC-BLYP, vertical ionization potentials (VIPs), vertical electron affinities (VEAs), bond lengths (R_e), vibrational frequency (ω_e) and binding energies (D_0) of dimers (Cu_2, CuNi and N_2) were calculated using LC-BLYP,[55] B3LYP,[57,58] BLYP,[57,59] B3PW91,[58,60] M06L,[61] M062X,[63] BHandHLYP,[62] PBEPBE,[45] PBEh1PBE,[63] PW91P86[64] and PW91PW91[65] methods with LANL2DZ basis sets. VIPs and VEAs were estimated from the highest occupied molecular orbital (HOMO) and the lowest unoccupied molecular orbital (LUMO) energies (ε_{HOMO} and ε_{LUMO}), as well as the energy difference of the neutral (E_N), cationic (E_C) and anionic states (E_A). An SCF=XQC option was used to converge self-consistent-field (SCF) calculations. The most stable copper clusters, Cu_n (n = 3-13), were obtained by geometry optimization for the reported most stable structures[20] with several possible spin multiplicities at the level of LC-BLYP/LANL2DZ. To search the lowest energy structures of the Ni-doped cluster Ni_mCu_{n-m} (m = 1, 2; n = 3-13), initial geometries were generated by substituting one or two Cu atoms in the most stable copper clusters with Ni (the number of geometries is a combination, ${}_nC_m$, for Ni_mCu_{n-m}), and geometry optimization was performed for all possible isomers with several possible spin states at the same level. Harmonic vibrational frequencies were computed to verify that the optimized structures have no imaginary frequency. All computations were performed using the Gaussian 16 package.[62]

Results and Discussion

Geometric Structures

Table 1 shows VIPs, VEAs, bond lengths, vibrational frequency and binding energies of Cu_2, CuNi and Ni_2, calculated by several methods. It is clearly shown that the LC-BLYP results are in best agreement with the experimental values,[66,67] indicating that LC-BLYP is the best choice for the current molecular systems. The spin multiplicity of the ground states of Cu_2, CuNi, and Ni_2 are verified to be singlet, doublet, and triplet, respectively. The relative energies of the dimers at different spin states are given in **Figure S1** (in supporting information). The calculated bond lengths of these dimers are in good agreement with the corresponding experimental values.[66,67] The Ni-Ni bond length in Ni_2 is shorter than the Cu-Cu in Cu_2 in the experiment, but the LC-BLYP result of Ni-Ni bond length is 0.02 Å longer than the Cu-Cu in Cu_2. This bond-length discrepancy is also reported in pervious theoretical studies,[41,66] which may be attributed to the presence of a lot of electronic states lying very close to the ground state. The Cu-Cu and Cu-Ni bond length differ with the corresponding experimental results by 0.00 Å and 0.02 Å, respectively, while the Ni-Ni distance is underestimated by 0.04 Å.

As far as the bond dissociation energies of Ni_2 dimer are concerned, M062X and BHandHLYP results show negative values. This simply implies that density functionals containing greater than or equal to 50% HF exchange predict wrong bond dissociation energies. It warrants the use of such DFT methods and an optimum balance of HF exchange in the DFT functional are essential for the study of the metal clusters.

Table 1. The VIPs, VEAs, equilibrium bond lengths, vibrational frequencies, and binding energies of Cu_2, CuNi and Ni_2 dimers, calculated by several functionals. The experimental values are also given.

Functional	VIP (eV)		VEA (eV)		R_e	ω_e	D_0
	$-\varepsilon_{HOMO}$	$E_C - E_N$	$-\varepsilon_{LUMO}$	$E_N - E_A$	(Å)	(cm^{-1})	(eV)
Cu-Cu Dimer							
LC-BLYP	7.66	7.6	0.42	0.45	2.22	282	1.87
BLYP	4.47	8.02	2.85	0.63	2.25	262	2.23
B3LYP	5.58	7.98	2.34	0.65	2.26	256	1.97
B3PW91	5.49	7.79	2.12	0.61	2.26	260	1.88
M06L	4.19	7.7	2.09	0.37	2.22	275	2.56
M062X	6.09	7.54	1.53	0.58	2.36	216	1.82
BHandHLYP	6.06	7.45	1.37	0.4	2.29	243	1.61
PBEPBE	4.48	7.98	2.79	0.69	2.25	267	2.27
PBEh1PBE	5.61	7.72	2	0.58	2.26	260	1.88
PW91P86	4.72	8.26	3.04	0.87	2.23	273	2.45
PW91PW91	4.57	8.07	2.86	0.72	2.24	269	2.3
Experiment[a)]	**7.9**				**2.22**	**264**	**2.01±0.08**
Cu-Ni Dimer							
LC-BLYP	7.61	7.38	0.46	0.5	2.25	276	1.72
BLYP	4.41	7.65	2.91	0.69	2.26	270	2.16
B3LYP	5.55	7.5	2.35	0.67	2.29	249	1.83
B3PW91	5.5	7.49	2.16	0.64	2.26	270	1.87
M06L	4.19	7.57	2.24	0.56	2.24	284	2.31
M062X	6	7.47	1.54	0.62	2.41	217	1.7
BHandHLYP	6	7.38	1.41	0.45	2.34	233	1.48
PBEPBE	4.41	7.66	2.85	0.75	2.25	276	2.25
PBEh1PBE	5.58	7.27	2.04	0.62	2.29	251	1.75
PW91P86	4.64	7.89	3.1	0.94	2.24	282	2.4
PW91PW91	4.49	7.71	2.92	0.79	2.24	278	2.27
Experiment[a)]	**7.36**				**2.23**	**273±1**	**2.05±0.10**
Ni-Ni Dimer							
LC-BLYP	7.61	7.41	0.44	0.5	2.24	300	1.88
BLYP	4.26	7.97	2.85	0.64	2.12	334	2.33
B3LYP	5.61	7.9	2.37	0.7	2.08	361	1.25
B3PW91	5.52	7.88	2.21	0.69	2.08	363	1.13
M06L	4.16	6.76	2.2	0.62	2.11	339	2.04

M062X	6.06	6.87	1.65	0.79	2.1	359	-0.61
BHandHLYP	6.12	6.33	1.53	0.61	2.05	392	-0.61
PBEPBE	4.29	7.57	2.83	0.77	2.12	336	2.57
PBEh1PBE	5.64	7.61	2.11	0.69	2.07	369	0.96
PW91P86	4.51	8.13	3.07	0.91	2.11	343	2.67
PW91PW91	4.38	8.13	2.9	0.77	2.11	339	2.56
Experiment[a)]	**7.36**				**2.20**	**280±20**	**2.068±0.01**

a) Refs. 66,67.

The optimized geometries of copper clusters, Cu_n (n = 3-13), in the ground state are presented with the electronic term in **Figure 1**. Note that Cu_3 to Cu_6 have 2D (two dimensional) structures, while Cu_7 to Cu_{13} have 3D (three dimensional) structures. The minimum and maximum Cu-Cu bond lengths (R_{min} and R_{max}, respectively) for each cluster size are shown in **Table 2**. As the cluster size grows, the Cu-Cu bond lengths increase ranging from 2.252 Å to 2.660 Å. It was found that the three-dimensional clusters approach to the experimental Cu-Cu distance of bulk, 2.556 Å.

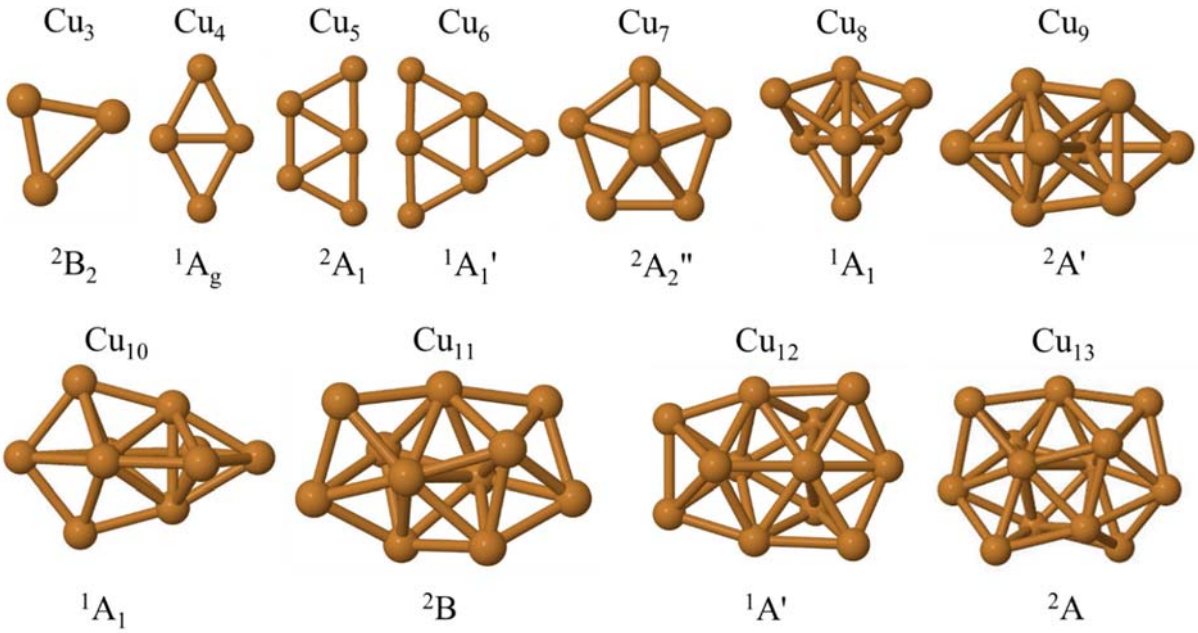

Figure 1. The lowest energy structures of the Cu_n (n = 3-13) clusters and their corresponding electronic states.

Table 2. The minimum and maximum bond lengths (R_{min}, R_{max}) in Å for the most stable structures of the Cu_n, $NiCu_{n-1}$ and Ni_2Cu_{n-2} (n = 3-13) clusters.

Cluster	Cu-Cu		Ni-Cu		Ni-Ni
	R_{min}	R_{max}	R_{min}	R_{max}	R
Cu_3	2.28	2.6			
Cu_4	2.25	2.4			
Cu_5	2.36	2.43			
Cu_6	2.36	2.43			
Cu_7	2.43	2.48			
Cu_8	2.43	2.45			
Cu_9	2.39	2.57			
Cu_{10}	2.41	2.53			
Cu_{11}	2.41	2.6			
Cu_{12}	2.38	2.66			
Cu_{13}	2.4	2.58			
$NiCu_2$	2.27	2.27	2.31	2.58	
$NiCu_3$	2.41	2.41	2.26	2.41	
$NiCu_4$	2.38	2.42	2.36	2.39	
$NiCu_5$	2.36	2.43	2.37	2.44	
$NiCu_6$	2.43	2.47	2.42	2.49	
$NiCu_7$	2.42	2.46	2.43	2.49	
$NiCu_8$	2.39	2.49	2.42	2.49	
$NiCu_9$	2.41	2.56	2.39	2.51	
$NiCu_{10}$	2.42	2.6	2.4	2.47	
$NiCu_{11}$	2.41	2.66	2.38	2.46	
$NiCu_{12}$	2.42	2.6	2.39	2.51	
Ni_2Cu			2.29	2.3	2.62
Ni_2Cu_2	2.39	2.39	2.27	2.41	2.42
Ni_2Cu_3	2.38	2.44	2.36	2.41	2.37
Ni_2Cu_4	2.35	2.35	2.37	2.43	2.12
Ni_2Cu_5	2.45	2.48	2.43	2.44	2.49
Ni_2Cu_6	2.44	2.47	2.43	2.45	2.53
Ni_2Cu_7	2.41	2.59	2.35	2.65	2.37
Ni_2Cu_8	2.43	2.57	2.39	2.48	2.43

Ni_2Cu_9	2.43	2.61	2.4	2.49	2.44
Ni_2Cu_{10}	2.42	2.65	2.4	2.54	2.45
Ni_2Cu_{11}	2.4	2.6	2.39	2.51	2.42

When a single Ni atom is doped into the most stable structure of Cu_n clusters, many isomers are possible. **Figure 2** shows the lowest energy optimized structures of the $NiCu_{n-1}$ clusters (n = 3-13) with their corresponding electronic terms. It is worth pointing out that $NiCu_{n-1}$ geometries are very similar to those of Cu_n (n = 3-13). In a case of copper clusters, odd-numbered clusters have the doublet and even-numbered clusters have the singlet ground state while the odd-numbered and even-numbered $NiCu_{n-1}$ (n = 3-13) clusters prefer to have the triplet and doublet spin states, respectively. In these clusters, mainly two different bond lengths (Ni-Cu and Cu-Cu) are obtained, and Table 2 shows that $NiCu_3$ has the minimum Ni-Cu bond length, 2.26 Å, and $NiCu_2$ has the maximum Ni-Cu bond length, 2.58 Å. On the other hand, the $NiCu_2$ has the shortest Cu-Cu bond length of 2.27 Å and the $NiCu_{11}$ cluster has the longest Cu-Cu bond length of 2.66 Å.

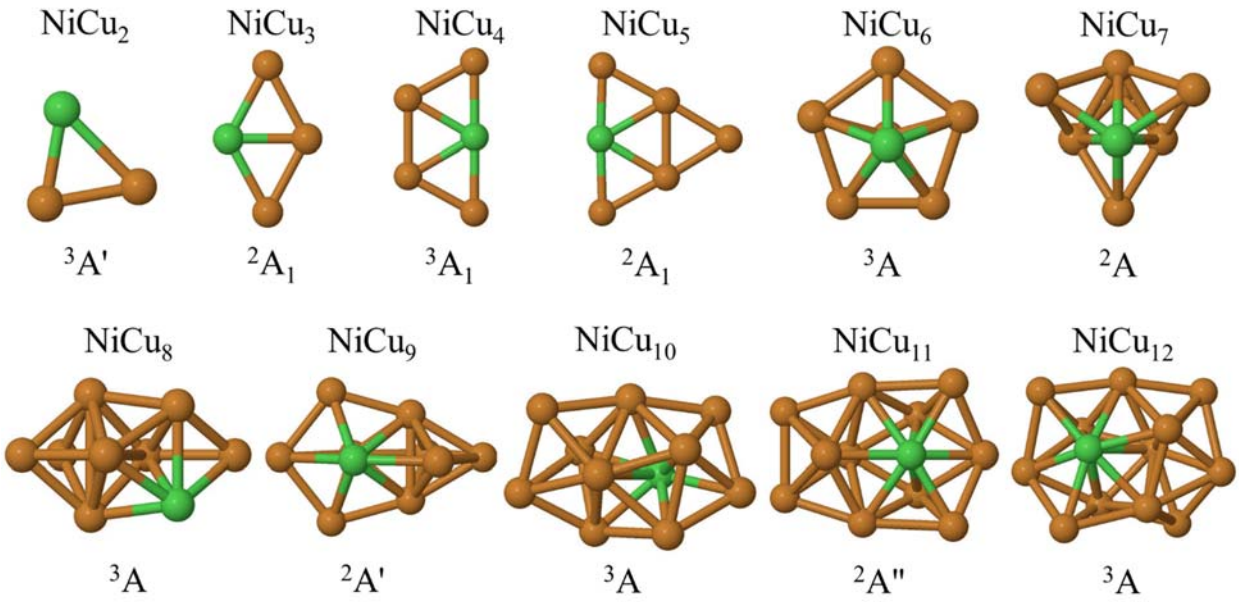

Figure 2. The lowest energy structures of the $NiCu_{n-1}$ (n = 3-13) clusters and their corresponding electronic states. The brown and green color represent Cu and Ni atom, respectively.

Figure 3 shows the most stable isomers for Ni_2Cu_{n-2} (n = 3-13) with the electronic terms, where two Ni atoms are doped to the most stable structure of Cu_n clusters. It is noted that geometries of Ni_2Cu_{n-2} are also similar to those of Cu_n. Here, Ni_2Cu, Ni_2Cu_3, Ni_2Cu_5, and Ni_2Cu_9 are quartet in the ground state, while Ni_2Cu_2, Ni_2Cu_4, Ni_2Cu_6, and Ni_2Cu_8 are triplet in the ground state. However, Ni_2Cu_7 and Ni_2Cu_{11} are doublet in the ground state, which is lying 0.03 eV below the quartet state, whereas Ni_2Cu_{10} is quintet with the triplet lying only 0.33 eV above and the septet is just 1.36 eV above the quintet. The relative energies of the clusters in different spin states are given in **Figures S2-S4** (in supporting information). In Table 2, three different types of bond lengths, namely, Ni-Ni, Ni-Cu and Cu-Cu are tabulated for Ni_2Cu_{n-2} (n = 3-13). The Ni-Ni bond length has the longest (2.62 Å) and shortest (2.12 Å) for Ni_2Cu and Ni_2Cu_4, respectively. In general, as the structure changes from 1D to 2D and from 2D to 3D, Ni-Ni bond lengths decrease while Ni-Cu bond lengths increase from 2.27 Å to 2.65 Å and the

Cu-Cu bond lengths change from 2.35 Å to 2.65 Å. The optimized parameters are compiled in **Tables S1-S3** (in supporting information).

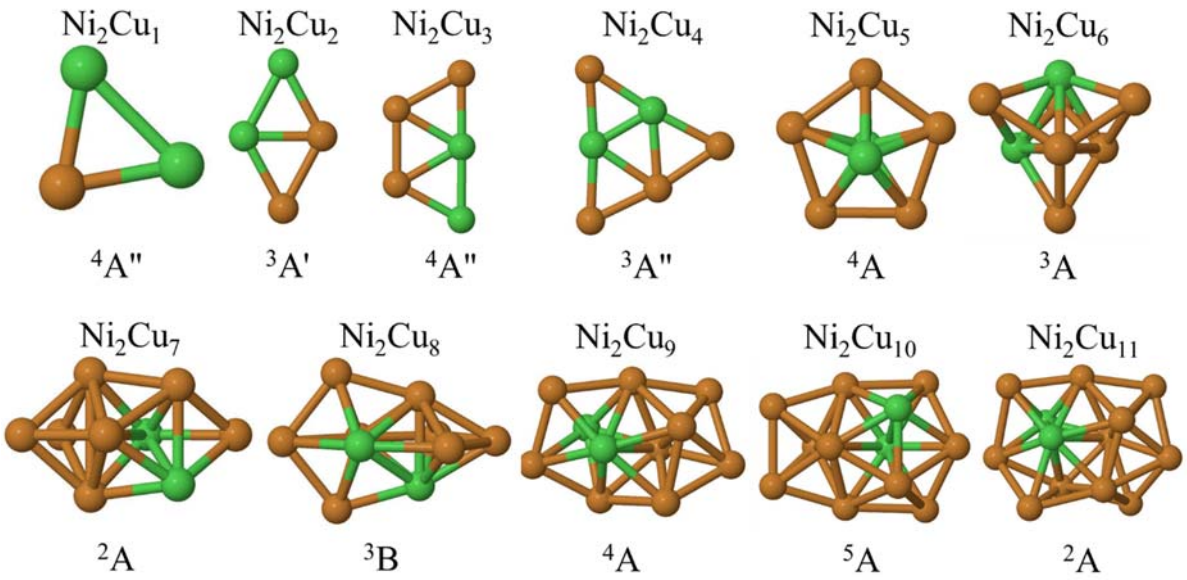

Figure 3. The lowest energy structures of the Ni_2Cu_{n-2} (n = 3-13) clusters and their corresponding electronic states. The brown and green color represent Cu and Ni atom, respectively.

Recently, Lin et al.[68] employed a combination of far-infrared multiple photon dissociation (FIR-MPD) spectroscopy and quantum chemical calculations to determine the structures of small isolated yttrium-doped gold clusters Au_nY (n = 1–9). Consequently, the computed vibrational spectra of the lowest energy Cu_n, $NiCu_{n-1}$ and Ni_2Cu_{n-2} (n = 2-13) clusters are shown in **Figure 4**. The Cu_2 and Ni_2 dimers have no absorption peaks because these dimers merely have a stretching vibration without change of a dipole moment. With regard to the clusters having planar or highly symmetrical geometries, the absorbed peaks are less than those of others. In case of Ni-doped copper clusters, the characteristic frequencies appeared in a higher region than the counter part of the pure copper clusters. The vibrational fundamentals of all the clusters are observed in the range of 5 to 350 cm^{-1}.

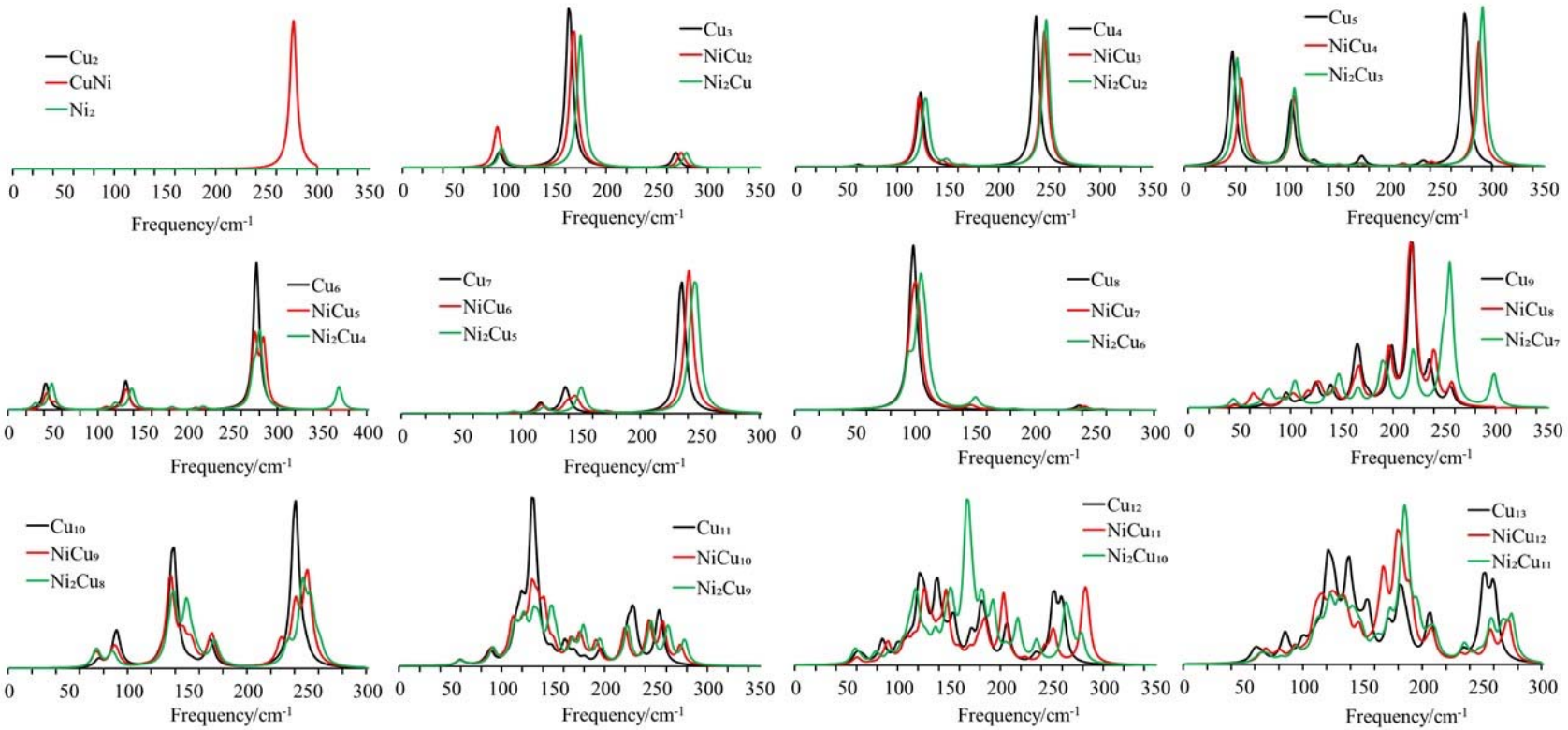

Figure 4. Computed vibrational spectra of the lowest energy structures of the Cu_n, $NiCu_{n-1}$ and Ni_2Cu_{n-2} (n = 2-13) clusters are plotted with 2 cm^{-1} infrared (IR) peak full width at half-height, and the peaks intensities have been extracted here in multiple of 10^{-40} esu^2 cm^2.

Relative Stabilities

In order to predict and compare the relative stabilities of the lowest energy structures of the clusters, it is significant to compute the binding energy per atom (E_{BE}). This can be defined as follows

$$E_{\mathrm{BE}}(\mathrm{Cu}_n) = \frac{nE_{\mathrm{Cu}} - E_{\mathrm{Cu}_n}}{n} \quad (1)$$

$$E_{\mathrm{BE}}(\mathrm{NiCu}_{n-1}) = \frac{(n-1)E_{\mathrm{Cu}} + E_{\mathrm{Ni}} - E_{\mathrm{NiCu}_{n-1}}}{n+1} \quad (2)$$

$$E_{\mathrm{BE}}(\mathrm{Ni_2Cu}_{n-2}) = \frac{(n-2)E_{\mathrm{Cu}} + 2E_{\mathrm{Ni}} - E_{\mathrm{Ni_2Cu}_{n-2}}}{n+2} \quad (3)$$

where E_{Cu}, E_{Cu_n}, E_{Ni}, $E_{\mathrm{NiCu}_{n-1}}$, $E_{\mathrm{Ni_2Cu}_{n-2}}$ denote the total energy of Cu atom, Cu_n, Ni atom, $NiCu_{n-1}$ and Ni_2Cu_{n-2}, respectively. The calculated binding energies per atom for the lowest energy structures of the Cu_n, $NiCu_{n-1}$ and Ni_2Cu_{n-2} clusters are shown in **Figure 5**. The results indicate that E_{BE} increases as a function of the number of atoms in clusters and at $n = 9$, the clusters possess relatively lower binding energies than the clusters at $n = 8$. E_{BE} of the single Ni-doped copper clusters is greater than E_{BE} of pure copper clusters, but lower than those of the doubly Ni-doped copper clusters. This implies that the doped clusters can continue to gain an energy during the growth process.

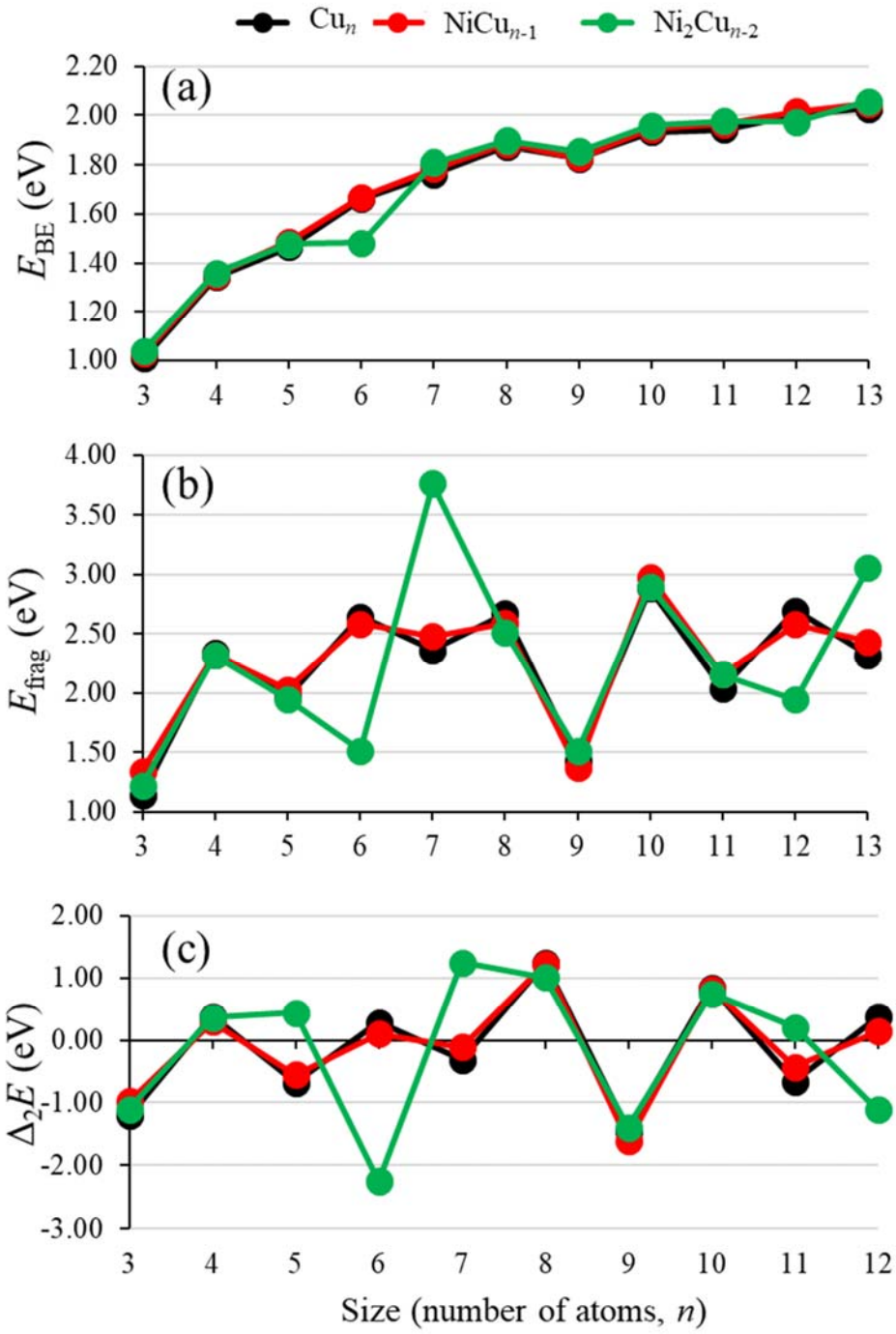

Figure 5. (a) Averaged binding energy (E_{BE}), (b) fragmentation energies (E_{frag}), and (c) size dependence of the second-order energy difference (Δ_2E) for the lowest energy structures of the Cu$_n$, NiCu$_{n-1}$ and Ni$_2$Cu$_{n-2}$ (n = 3-13) clusters.

Another parameter to understand the stability of the cluster is the fragmentation energies (E_{frag}). Fragmentation processes may involve dissociation barriers. However, from a purely energetic point of view, the fragmentation energies (E_{frag}) of the most stable clusters can be expressed as

$$E_{\mathrm{frag}}(\mathrm{Cu}_n) = E_{\mathrm{Cu}_{n-1}} + E_{\mathrm{Cu}} - E_{\mathrm{Cu}_n} \quad (4)$$

$$E_{\mathrm{frag}}(\mathrm{NiCu}_{n-1}) = E_{\mathrm{NiCu}_{n-2}} + E_{\mathrm{Cu}} - E_{\mathrm{NiCu}_{n-1}} \quad (5)$$

$$E_{\mathrm{frag}}(\mathrm{Ni_2Cu}_{n-2}) = E_{\mathrm{Ni_2Cu}_{n-3}} + E_{\mathrm{Cu}} - E_{\mathrm{Ni_2Cu}_{n-2}} \quad (6)$$

Where $E_{\mathrm{Cu}_{n-1}}$ and $E_{\mathrm{Ni_2Cu}_{n-3}}$ are the total energy of the Cu_{n-1} and Ni_2Cu_{n-3} clusters, respectively. When the fragmentation energies are negative, the parent clusters are unstable and could dissociate spontaneously by releasing an energy of $|E_{frag}|$. In this work, all the clusters have positive fragmentation energies, implying that the parent clusters are stable and one must supply energy to induce fragmentations. Generally, a higher fragmentation energy leads to lower the stability of the cluster.

The E_{frag} values for the lowest energy structures of Cu_n, $NiCu_{n-1}$ and Ni_2Cu_{n-2} as a function of cluster size are shown in **Figure 5**. It is found that the Cu_3, $NiCu_2$ and Ni_2Cu clusters have the lowest fragmentation energies while Cu_{10}, $NiCu_9$ and Ni_2Cu_5 have the largest fragmentation energies of 2.88 eV, 2.98 eV and 3.76 eV, respectively.

In cluster physics, the second–order energy difference (Δ_2E) is used to measure the relative stabilities of the most stable clusters. For Cu_n, $NiCu_{n-1}$ and Ni_2Cu_{n-2} clusters in the ground state, Δ_2E can be calculated as

$$\Delta_2 E_{\mathrm{Cu}_n} = E_{\mathrm{Cu}_{n-1}} + E_{\mathrm{Cu}_{n+1}} - 2E_{\mathrm{Cu}_n} \quad (7)$$

$$\Delta_2 E_{\mathrm{NiCu}_{n-1}} = E_{\mathrm{NiCu}_{n-2}} + E_{\mathrm{NiCu}_n} - 2E_{\mathrm{NiCu}_{n-1}} \quad (8)$$

$$\Delta_2 E_{Ni_2Cu_{n-2}} = E_{Ni_2Cu_{n-3}} + E_{Ni_2Cu_{n-1}} - 2E_{Ni_2Cu_{n-2}} \quad (9)$$

where E is the total energy of the ground-state clusters. The calculated second-order energy differences as a function of the cluster size are illustrated in **Figure 5**. It is obvious that the even-numbered clusters are more stable than the odd-numbered ones. However, the introduction of two Ni atoms into copper cluster alters the stability pattern of the host clusters significantly for the $5 \leq n \leq 7$ and $n = 11, 12$. Therefore, three maxima are observed for Ni_2Cu_3, Ni_2Cu_5 and Ni_2Cu_6 clusters.

HOMO-LUMO Gaps and Charge Transfer

The HOMO-LUMO gap is an important parameter to examine the chemical stability of the clusters. A large energy gap usually correlates with remarkable kinetic stability. The calculated values of the HOMO-LUMO energy gaps for the lowest energy structures of Cu_n, $NiCu_{n-1}$ and Ni_2Cu_{n-2} clusters are plotted in **Figure 6**. It is interesting to notice that the energy gap trends are similar in all three cases with exceptions of Ni_2Cu_{10} and Ni_2Cu_{11} clusters. The chemical inertness increases from 1D to 2D clusters and then keeps decreasing as structural transitions from 2D to 3D clusters. The clusters containing seven atoms seem unique by showing more reactiveness among the clusters having *n* values in the range of 2 to 8 because of highly symmetric geometry. However, the Ni-atom doping into the copper clusters reduces the chemical inertness and the results show that copper clusters doped with two Ni-atoms are more reactive than those doped with a single Ni-atom and pure copper clusters. In the pure copper clusters, there is observed odd-even alternation in the HOMO-LUMO energy gaps because of the electron pairing effect. Moreover, in Ni_2-doped copper clusters case, quartet, triplet and quintet are the ground states while in single Ni-doped copper cluster, doublet and triplet are the most stable spin states for even-numbered and odd-numbered clusters, respectively. It means that higher spin states make the HOMO-LUMO gap narrower, and so Ni_2Cu_{10} is the most reactive clusters because its spin state in the ground state is quintet. Similarly, the clusters with $n = 6$ are the most inert clusters.

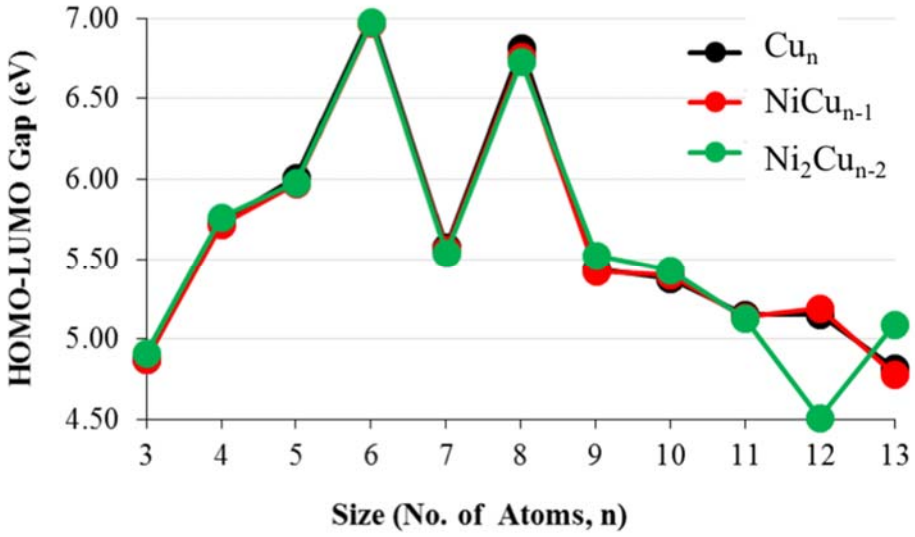

Figure 6. HOMO-LUMO gap of the lowest energy structures of the Cu_n, $NiCu_{n-1}$ and Ni_2Cu_{n-2} (n = 3-13) clusters.

The natural charges obtained in natural bond orbital (NBO) analyses[69] for Ni-doped copper clusters can provide a reliable charge-transfer information. Here, natural charges of the dimers and Ni atoms in the most stable $NiCu_{n-1}$ and Ni_2Cu_{n-2} clusters were investigated. The calculated results are listed in **Table S4**. For the dimers case, Cu_2 and Ni_2 are neutral but in CuNi dimer, Cu and Ni atoms bear negative and positive charge of the same magnitude, respectively. It indicates that the charge transfer takes place from Ni atom to Cu atom though Ni atom has the larger electronegativity than that of the Cu atom. To make it clear, the natural electronic configurations given in **Table S4** illustrate that Ni-4s orbital donates charge to Cu-4s orbital, making it an electron acceptor. On the contrary, charges are transferred from Cu atoms to the Ni atoms in Ni-doped copper clusters of size larger than a dimer.

Electronic Properties

The vertical ionization potential (VIP) and the vertical electron affinity (VEA) are two important factors to get insight into the electronic property and can be calculated as follows

$$\mathrm{VIP} = E_{\mathrm{cation}} - E_{\mathrm{neutral}} \qquad (10)$$

$$\mathrm{VEA} = E_{\mathrm{neutral}} - E_{\mathrm{anion}} \qquad (11)$$

Where E_{cation} and E_{anion} are energies of the cationic and anionic systems, respectively, calculated at the optimized geometry of the neutral system with the energy E_{neutral}. By introducing E_{HOMO} (HOMO energy) and E_{LUMO} (LUMO energy), the above equations can be rewritten using the Janak's theorem[70] and the linearity condition for orbital energies[71] as

$$\mathrm{VIP} = -E_{\mathrm{HOMO}} = E_{\mathrm{cation}} - E_{\mathrm{neutral}} \qquad (12)$$

$$\mathrm{VEA} = -E_{\mathrm{LUMO}} = E_{\mathrm{neutral}} - E_{\mathrm{anion}} \qquad (13)$$

According to these equations, VIP and VEA were calculated for the lowest energy Cu_n, $NiCu_{n-1}$ and Ni_2Cu_{n-2} clusters, which are shown in **Table 3**, along with the available experimental data. As an overall, the calculated VIPs of pure copper clusters show a very good agreement with the experimental values.[72,73] HOMO and LUMO energies are a measure of the accuracy of DFT methods, and in this context, the excellent agreement for VIP and VEA confirms the reliability of the results. This indicates that the orbital energies by LC-DFT are reliable and can be used to predict the VIP and VEA. For odd-numbered clusters, the energy of LUMO for β-spin orbital represents VEA.

Table 3. Vertical ionization potential (VIP) and vertical electron affinity (VEA) of the lowest energy structures for the Cu_n, $NiCu_{n-1}$ and Ni_2Cu_{n-2} (n = 3-13) clusters. Here E_N, E_C and E_A represent the total energies of neutral, cation and anion clusters, respectively.

Clusters	VIP (eV)			VEA (eV)	
	E_C-E_N	–HOMO	Exp [a)]	E_N-E_A	–LUMO
Cu_3	5.53	5.63	5.80±0.05	0.92	0.76
Cu_4	6.32	6.52	7.15±0.75	0.96	0.78
Cu_5	6.03	6.31	6.30±0.05	1.28	1.07
Cu_6	7.06	7.45	7.15±0.75	0.64	0.44
Cu_7	5.65	5.95	6.07±0.05	1.22	0.95
Cu_8	6.85	7.27	7.15±0.75	0.61	0.46
Cu_9	5.85	6.16	5.36±0.05	1.72	1.42
Cu_{10}	5.67	6.01	6.07±0.05	0.89	0.63
Cu_{11}	5.62	5.96	5.91±0.05	1.73	1.43
Cu_{12}	5.91	6.3	6.30±0.05	1.44	1.14
Cu_{13}	5.34	5.7	5.66±0.05	1.7	1.38
Ni_2Cu	5.52	5.66		0.91	0.74
Ni_2Cu_2	7.75	6.51		0.92	0.75
Ni_2Cu_3	5.92	6.28		1.29	1.01
Ni_2Cu_4	5.84	7.4		1.52	0.22
Ni_2Cu_5	5.56	5.87		1.09	0.82
Ni_2Cu_6	6.51	7.16		0.17	0.43
Ni_2Cu_7	5.61	6.69		1.48	1.16
Ni_2Cu_8	5.56	6.02		0.89	0.53
Ni_2Cu_9	5.51	5.85		1.64	1.27
Ni_2Cu_{10}	4.98	5.35		2.09	1.66
Ni_2Cu_{11}	7.17	6.39		1.63	1.3
$NiCu_2$	5.51	5.63		0.92	0.75
$NiCu_3$	6.3	6.49		0.95	0.73
$NiCu_4$	6.26	6.27		1.22	1.01

$NiCu_5$	7.14	7.4		0.63	0.43
$NiCu_6$	5.61	5.91		1.18	0.88
$NiCu_7$	6.56	7.2		0.61	0.42
$NiCu_8$	5.8	6.13		1.75	1.36
$NiCu_9$	7.82	6.02		0.99	0.59
$NiCu_{10}$	5.56	5.9		1.68	1.33
$NiCu_{11}$	5.56	6.31		1.54	1.04
$NiCu_{12}$	5.29	5.65		1.67	1.28

[a)] Refs. 72, 73.

Reactivity Descriptors

In conceptual density functional theory, chemical potential (μ), chemical hardness (η) and electrophilicity index (ω) are indicators of the reactivity and stability.[74] All of these are well established to represent global quantities in chemical reactivity and our interests here to exploit these concepts to rationalize the behavior of the clusters. Using a finite difference method [75] and Koopmans theorem[76], the formal expressions for chemical potential, chemical hardness and electrophilicity index are

$$\mu = \frac{-\mathrm{VIP}-\mathrm{VEA}}{2} = \frac{\mathrm{HOMO} + \mathrm{LUMO}}{2} \qquad (14)$$

$$\eta = \frac{\mathrm{VIP} - \mathrm{VEA}}{2} = \frac{\mathrm{LUMO} - \mathrm{HOMO}}{2} \qquad (15)$$

$$\omega = \frac{\mu^2}{\eta} \qquad (16)$$

The chemical potential measures the escaping tendency of the electrons from a system; the charge transfer from the higher μ of a system to the lower μ of another system takes place until the chemical potential becomes constant through the space. The chemical potential, derived from equation (14), for the lowest energy Cu_n, $NiCu_{n-1}$ and Ni_2Cu_{n-2} (n = 3-13) clusters are presented in **Table 4**. The chemical potential calculated on the basis of HOMO and the LUMO energies are given in the bracket. It is expected that the open-shell clusters will have maximum values of μ and after one electron transfer, these systems will have a closed-shell, and the resulting systems will be more stable than the original open-shell clusters. In general, Table 5 shows that the odd-number open-shell clusters present higher values of μ than the even closed-shell neighboring clusters. Similar trends are observed in all three kinds of clusters. When Cu atoms are replaced by Ni atoms, then the chemical potential of the clusters decrease with those of the pure copper clusters of the same size. However, some abnormal chemical potential, calculated on the basis of VIP and VEA

values, were observed for Ni_2Cu_2 and $NiCu_9$ clusters. We attribute this discrepancy due to somewhat overestimated total energies of the anionic clusters given by DFT methods. Overall, the Ni_2Cu_{11} cluster has the lowest chemical potential and the clusters containing three atoms have the highest chemical potential. These results also seem to show that the chemical potential of the clusters calculated from HOMO and LUMO energies are in close agreement with those of the chemical potential derived from VIP and VEA. Therefore, HOMO and LUMO energies obtained by LC-DFT can be directly used not only to predict the chemical potential of the systems but also to check the correct values of VIP and VEA of the systems.

Table 4. Chemical potential (μ), chemical hardness (η) and electrophilicity index (ω) of the lowest energy structures of the Cu_n, $NiCu_{n-1}$ and Ni_2Cu_{n-2} (n = 3-13) clusters, using the VIP and VEA values. The results in brackets were obtained using the HOMO and LUMO energies.

	Chemical Potential (eV)		
n	Cu_n	$NiCu_{n-1}$	Ni_2Cu_{n-2}
3	-3.22 (-3.20)	-3.22 (-3.19)	-3.14 (-3.20)
4	-3.64 (-3.65)	-3.63 (-3.61)	-4.33 (-3.63)
5	-3.65 (-3.69)	-3.74 (-3.64)	-3.61 (-3.65)
6	-3.85 (-3.95)	-3.88 (-3.91)	-3.68 (-3.81)
7	-3.43 (-3.45)	-3.40 (-3.40)	-3.33 (-3.34)
8	-3.73 (-3.87)	-3.58 (-3.81)	-3.34 (-3.79)
9	-3.79 (-3.79)	-3.77 (-3.75)	-3.55 (-3.93)
10	-3.28 (-3.32)	-4.40 (-3.30)	-3.22 (-3.27)
11	-3.68 (-3.69)	-3.62 (-3.62)	-3.57 (-3.56)
12	-3.68 (-3.72)	-3.55 (-3.67)	-3.53 (-3.51)
13	-3.52 (-3.54)	-3.48 (-3.46)	-4.40 (-3.85)

	Chemical Hardness (eV)

n	Cu_n	$NiCu_{n-1}$	Ni_2Cu_{n-2}
3	2.31 (2.44)	2.29 (2.44)	2.39 (2.46)
4	2.68 (2.87)	2.67 (2.88)	3.41 (2.88)
5	2.38 (2.62)	2.52 (2.63)	2.31 (2.64)
6	3.21 (3.50)	3.26 (3.49)	2.16 (3.59)
7	2.22 (2.50)	2.21 (2.51)	2.23 (2.53)
8	3.12 (3.41)	2.98 (3.39)	3.17 (3.36)
9	2.07 (2.37)	2.03 (2.38)	2.07 (2.76)
10	2.39 (2.69)	3.41 (2.72)	2.34 (2.75)
11	1.94 (2.27)	1.94 (2.29)	1.94 (2.29)
12	2.23 (2.58)	2.01 (2.64)	1.44 (1.84)
13	1.82 (2.16)	1.81 (2.18)	2.77 (2.55)

	Electrophilicity Index (eV)		
n	Cu_n	$NiCu_{n-1}$	Ni_2Cu_{n-2}
3	2.25 (2.09)	2.26 (2.09)	2.07 (2.09)
4	2.47 (2.32)	2.46 (2.26)	2.75 (2.29)
5	2.81 (2.60)	2.78 (2.52)	2.81 (2.53)
6	2.31 (2.22)	2.32 (2.20)	3.13 (2.02)
7	2.66 (2.38)	2.61 (2.30)	2.48 (2.21)
8	2.23 (2.19)	2.16 (2.14)	1.76 (2.14)
9	3.47 (3.03)	3.51 (2.95)	3.04 (2.79)
10	2.25 (2.05)	2.84 (2.01)	2.22 (1.95)
11	3.47 (3.01)	3.37 (2.86)	3.30 (2.77)
12	3.03 (2.69)	3.14 (2.56)	4.33 (3.34)
13	3.40 (2.91)	3.35 (2.75)	3.49 (2.91)

The chemical hardness is a global molecular property and provides information about general feature of a reactive molecule. Therefore, the chemical hardness, η, of the most stable Cu_n, $NiCu_{n-1}$ and Ni_2Cu_{n-2} (n = 3-13) clusters are calculated using equation (15) which are listed in **Table 4**. The results obtained from HOMO and LUMO are shown inside the bracket. From **Table 4**, one can observe that the even-numbered clusters have higher values of hardness than their odd-

numbered neighboring clusters. These trends are also similar to the fragmentation energy and the HOMO-LUMO energy gap trends as mentioned-above. In general, Ni-doping makes the clusters more inert against the host clusters. In addition, Cu_{13}, $NiCu_{12}$ and Ni_2Cu_{10} clusters show the lowest chemical hardness in Cu_n, $NiCu_{n-1}$ and Ni_2Cu_{n-2} (n = 3-13) clusters, respectively.

The electrophilicity index, ω, is another parameter to measure the electrophilic power of a system, just as, in classical electrostatics, power = V^2/R, and μ and η serve the purpose of potential (V) and resistance (R), respectively. The relation among ω, μ and η are shown in equation (16). The computed ω for the clusters are given in **Table 4**. The results show that the Ni_2Cu_{10} and Ni_2Cu_6 clusters have the highest and the lowest electrophilicity index, respectively. The Ni-doping into copper clusters affects the electrophilic power of the pure copper clusters. We have also checked the minimum electrophilicity principle[77-79] for a small cluster containing three atoms, $NiCu_2$, as given below in **Table 5**. This result indicates that the more stable structure has the lower electrophilicity value, hence the minimum electrophilicity principle is satisfied.

Table 5. The electrophilicity values for the $NiCu_2$ clusters.

Triplet state	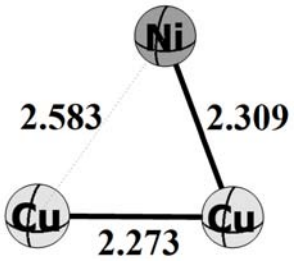	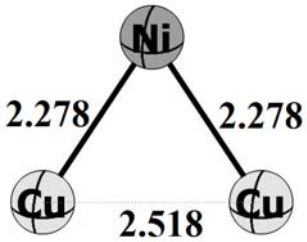
Symmetry	C_s	C_{2v}
Total energy (a.u.)	-560.916304	-560.915046
− HOMO (eV)	5.63	5.59
− LUMO (eV)	0.75	0.77
η (eV)	2.44	2.41
μ (eV)	-3.19	-3.18
ω (eV)	4.178	4.204

Polarizability and the Minimum Polarizability Principle (MPP)

The static polarizability is considered as one of the most important observables to measure the distortion of the electron density under the effect of an external static electric field. The average static polarizability, $<\alpha>$, is defined as[74]

$$< \alpha > = (\alpha_{xx} + \alpha_{yy} + \alpha_{zz})/3 \qquad (17)$$

In **Table 6** we show the averaged static polarizability of the lowest energy structures of the Cu_n, $NiCu_{n-1}$ and Ni_2Cu_{n-2} (n = 3-13) clusters using equation (17). We note that as going from n = 3 to n = 13, the averaged static polarizability increases. The Ni-doping into pure copper clusters increases $<\alpha>$ from n = 3 to n = 8 while opposite trends are observed from n = 9 to n = 13. All in all, the Cu_{13} cluster has the largest averaged static polarizability followed by $NiCu_{12}$ and Ni_2Cu_{11} clusters and Cu_3 has the lowest averaged static polarizability.

Table 6. The averaged static polarizability,$< \alpha >$, in atomic units of the lowest energy structures of the Cu_n, $NiCu_{n-1}$ and Ni_2Cu_{n-2} (n = 3-13) clusters.

	$< \alpha >$ (au)		
n	Cu_n	$NiCu_{n-1}$	Ni_2Cu_{n-2}
3	142.69	145.23	147.30
4	147.97	149.95	150.97
5	189.08	191.35	194.73
6	206.74	210.29	206.81
7	240.13	240.45	241.53
8	259.98	260.39	260.56
9	307.16	309.71	304.12
10	330.35	331.22	330.43
11	365.09	362.69	363.00
12	385.54	384.22	406.87
13	420.43	417.77	415.07

In order to show the consistency between the energetics and electronic descriptors, we show a good linear relation between the binding energies per atom, E_{BE}, and the average static polarizability per atom, $<\alpha>/n$, of the Cu_n, $NiCu_{n-1}$ and Ni_2Cu_{n-2} (n = 3-13) clusters in **Figure 7** . The results show that Cu_{13}, $NiCu_{12}$ and Ni_2Cu_{11} clusters have the largest E_{BE} with minimum $<\alpha>/n$ values in their corresponding classes of the clusters. Overall, Ni_2Cu_{11} cluster has the largest averaged binding energies of 2.06 eV at the lowest averaged static polarizability per atom value of 31.93 a.u. amongst all three kinds of clusters. This indicates that the clusters with strong bonds (or high electronic delocalization degree) present minimum values of a polarizability per atom, in agreement with the minimum polarizability principle (MPP) which states that[74] 'the natural direction of evolution of any system is towards a state of minimum polarizability.'

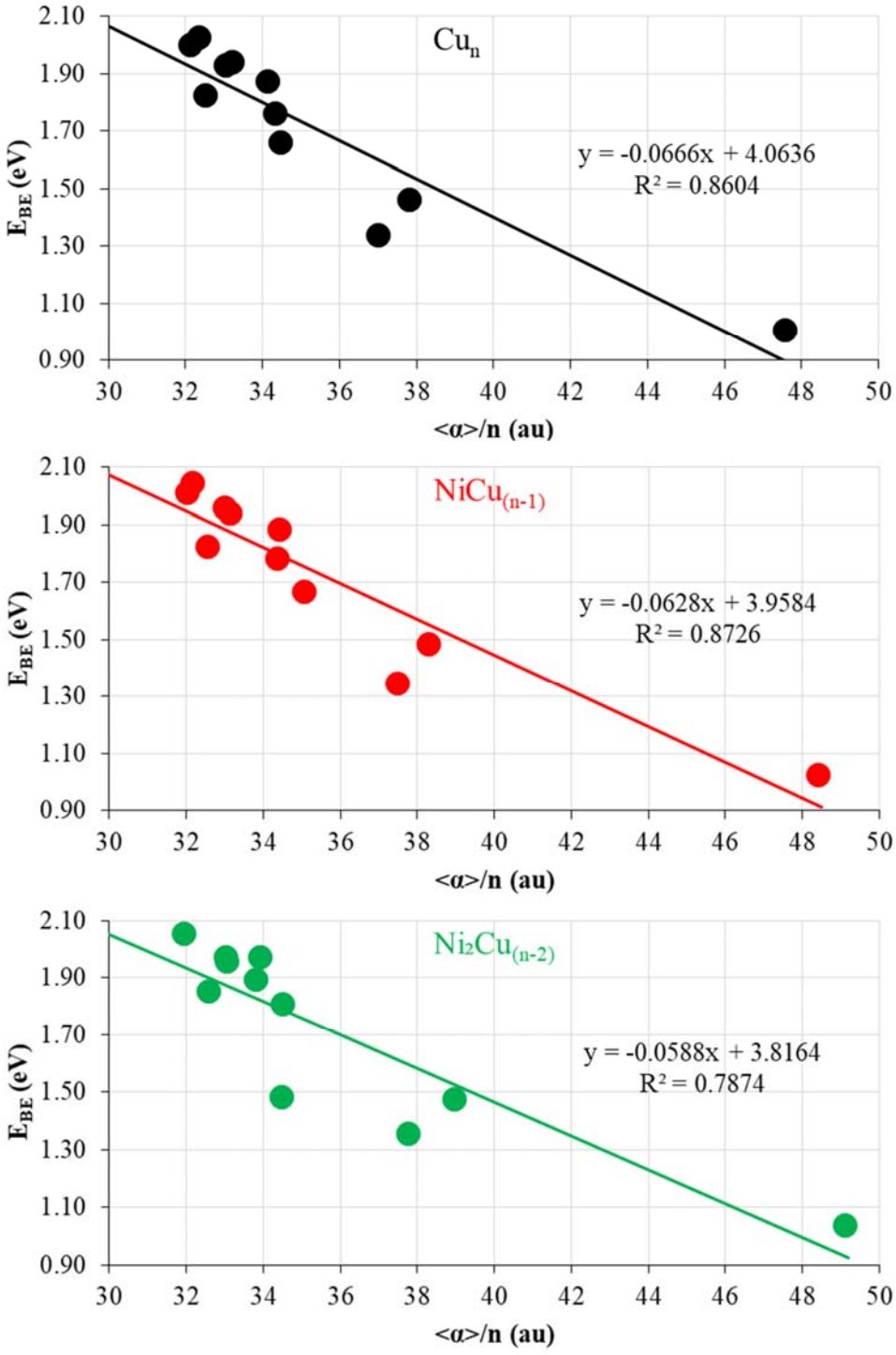

Figure 7. Correlation between the averaged binding energy (E_{BE}) and the averaged static polarizability per atom (<α>/n) of the Cu$_n$, NiCu$_{n-1}$ and Ni$_2$Cu$_{n-2}$ (n = 3-13) clusters.

Magnetic Properties

The magnetic properties of the metal clusters are always important to make nano-electronic devices and high density magnetic storage materials. The total magnetic moment (μ_{tot}) in the Russel-Saunders scheme is a combination of a total spin magnetic moment (S) and a total orbital magnetic moment (L) which is defined as $\mu_{tot} = (2S + L)\ \mu_B$ (μ_B is the Bohr magneton). In the Heisenberg model, one neglects the L contribution and then $\mu_{tot} = g_e\mu_B S$, where the gyromagnetic ratio g_e is 2.0023. Therefore, we consider the total magnetic moment, $\mu_{tot} = 2S\ \mu_B$, to be equal to the $[n_\alpha - n_\beta]\ \mu_B$, where n_α and n_β are the total numbers of the up-spin and the down-spin, respectively.

The total magnetic moments and total magnetic moments per atom calculated for the lowest energy Cu_n, $NiCu_{n-1}$ and Ni_2Cu_{n-2} (n = 3-13) clusters are displayed in **Figure 8**. The lowest energy copper clusters show an odd-even alternation as a function of the cluster size, n, in the total magnetic moment. The magnetic moment for Cu_n clusters with even n is completely quenched. For the single Ni-atom doped clusters, the magnetic moment is non-zero and is larger than that of the Cu_n clusters. In case of the doubly Ni-atoms doped copper clusters, the magnetic moments become larger than that of $NiCu_{n-1}$ clusters. However, for larger clusters, Ni_2Cu_7 and Ni_2Cu_{11}, the magnetic moment is equal to the magnetic moment of the Cu_9 and Cu_{13} clusters, respectively, due to the preferred singlet spin state. The Ni_2Cu_{10} cluster show the highest magnetic moment as it prefers the lowest energy in quintet spin state. In general, this result indicates that the substitution of Ni-atoms for Cu-atoms can enhance the magnetism of the host clusters.

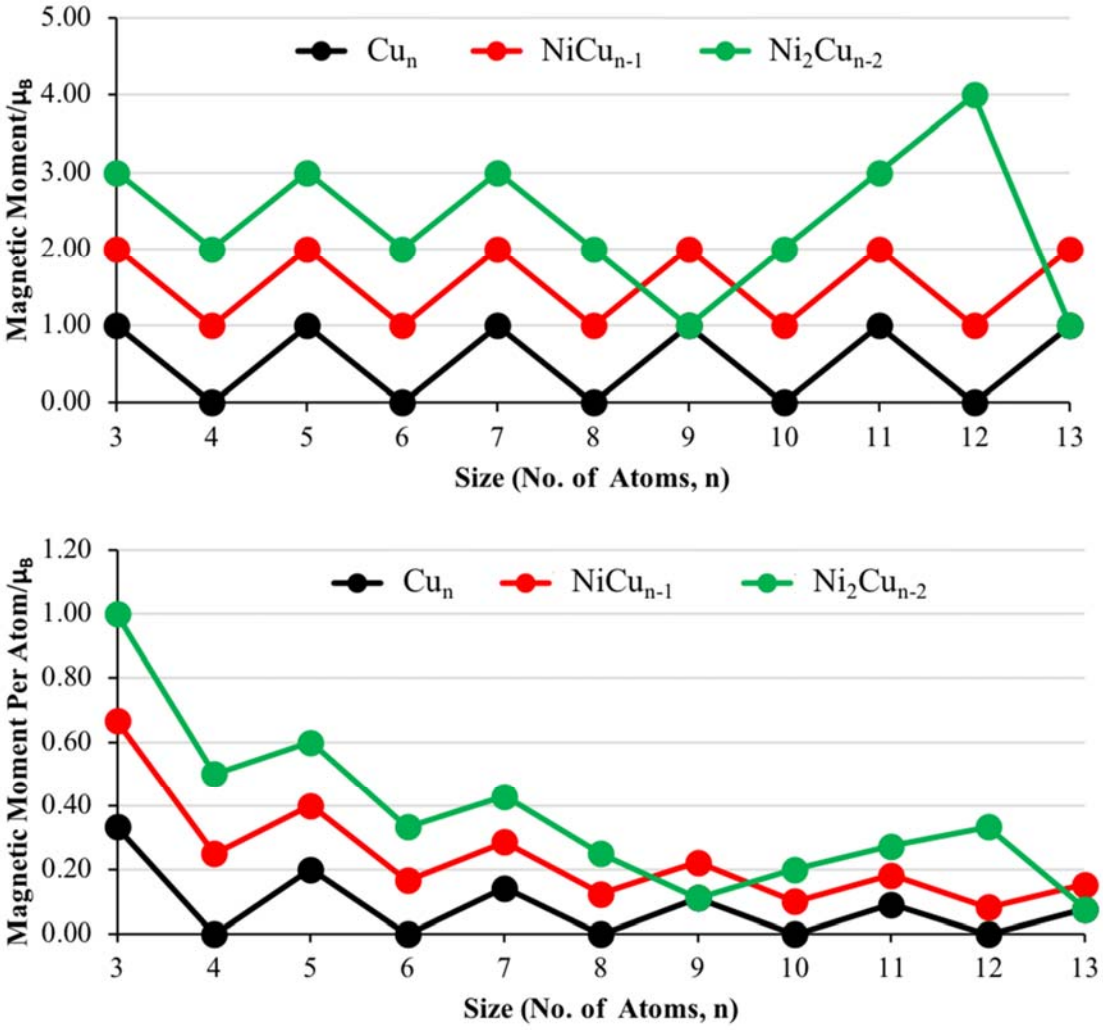

Figure 8. Size dependence of the total spin magnetic moment and the total spin magnetic moment per atom of the lowest energy structure for of the Cu_n, $NiCu_{n-1}$ and Ni_2Cu_{n-2} (n = 3-13) clusters.

Conclusion

In this work, we have systematically investigated geometric structures, relative stabilities, electronic structures, reactivity descriptors and magnetic properties of the single and double Ni atoms doped into the ground-state structures of the Cu_n (n = 3-13) clusters at the LC-BLYP/LANL2DZ level.

Firstly, we searched the lowest energy structures of Ni doped copper clusters by doping one or two Ni atoms to the lowest energy structures of Cu_n with all possible atomic positions and possible spin multiplicities, followed by geometry optimizations. The most stable structures revealed that Cu-Cu, Ni-Cu and Ni-Ni bond lengths increase as the size of the clusters grows and approaches to the experimental bulk metal distance. The computed vibrational spectra were presented to identify the most stable structures.

In order to understand the relative stabilities of the clusters, the binding energy per atom, the fragmentation energies and the second-order energy differences were computed. It was found that Ni_2-doped copper clusters and pure copper clusters have the highest and lowest binding energies per atom, respectively. These results signified that Ni-doped clusters can continue to gain an energy during the growth process. The positive fragmentation energies ensured that all the clusters are stable and Cu_{10}, $NiCu_9$ and Ni_2Cu_5 have the largest fragmentation energies in their corresponding classes of the clusters. The second-order energy differences indicated that the even-numbered clusters are more stable than the odd-numbered ones. All in all, the results showed that Ni_2Cu_{11} cluster is the most stable one among Cu_n, $NiCu_{n-1}$ and Ni_2Cu_{n-2} (n = 3-13) clusters.

The HOMO-LUMO gap showed an oscillating behavior with the cluster size increasing. The substitution of Cu by Ni in the copper clusters enhances the chemical reactivity of large

clusters and Ni_2Cu_{10} is the most reactive one. On the basis of the calculated natural charges from the NBO calculation, it was noticed that charges are transferred from Cu to Ni atoms.

Next we investigated the electronic properties of the clusters, i.e., vertical ionization potential and vertical electron affinity. The VIPs calculated from HOMO energies give excellent agreement with the experimental values while the LUMO energy gives well correspondence with VEA values obtained from the energies of neutral and anionic clusters. These results revealed that HOMO and LUMO energies from LC-DFT calculations are reliable and can be used to predict the VIP and VEA of systems for which experimental results are not available.

The reactivity descriptors, such as chemical potential, chemical hardness and electrophilicity index, are useful tools to get insights to more complex systems involved in heterogeneous catalysis and in cluster's fragmentation reactions. Ni_2Cu_{11} cluster has the lowest chemical potential while Cu_{13}, $NiCu_{12}$ and Ni_2Cu_{10} clusters show the lowest chemical hardness in Cu_n, $NiCu_{n-1}$ and Ni_2Cu_{n-2} clusters, respectively. Moreover, Ni_2Cu_{10} and Ni_2Cu_6 clusters have the highest and the lowest electrophilicity index, respectively. The results show that Ni-doping into copper clusters affects the chemical potential, chemical hardness and electrophilic power of the pure copper clusters.

Moreover, we also found that the more stable cluster has the lesser static polarizability in average. For example, Ni_2Cu_{11} cluster has the highest binding energies with the lowest static polarizability per atom, which is in agreement with MPP. This showed that the minimum polarizability principle is operative in the characterization of these clusters. We have also checked the minimum electrophilicity principle for $NiCu_2$ isomers, and found that the more stable isomer has the smaller electrophilicity value.

Finally, the total spin magnetic moment of Cu_n, $NiCu_{n-1}$ and Ni_2Cu_{n-2} clusters have been computed and Ni_2Cu_{10} cluster has the highest magnetic moment due to the lowest energy in quintet spin state. In general, the results indicated that the substitution of Cu-atoms with Ni-atoms in Cu_n clusters has conserved most of total spin magnetic moments. Based on these results, we conclude that long-range exchange interactions play a significant role in the study of metal clusters.

Supporting Information

The Supporting Information is available free of charge on the ACS Publications website at DOI: the optimized parameters, relative energies of the clusters in different spin states of the Ni_mCu_{n-m} (m = 0-2; n = 3-13) clusters etc.

Acknowledgment

The present work was partially supported by the MEXT program "Elements Strategy Initiative to Form Core Research Center", and the MEXT program "Priority Issue on Post-K computer" (Development of new fundamental technologies for high-efficiency energy creation, conversion/storage and use). T.I. and T.T. thank the financial support for JSPS KAKENHI Grant No. 17K14428 and 16KT0047, respectively. A part of calculations was performed using the Research Center for Computational Science, Okazaki, Japan.

References

(1) K. Philippot, P. Serp, Concepts in Nanocatalysis. In Nanomaterials in Catalysis; Wiley-VCH Verlag GmbH & Co. KGaA, **2013**; pp 1–54.

(2) A. T. Bell, G. C. Bond, D. T. Thompson, M. Valden, X. Lai, D. W. Goodman, T. Blasko, J. M. L. Nieto, K. Chen, A. T. Bell, E. Iglesia, T. Koyama, T. Komaya, P. L. Gai, M. Weyland, G. Durscher, N. D. Browning, S. J. Pennycook, F. Besenbacker, P. C. Thune, J. Loss, D. Wonter, P. J. Leustra, J. W. Niemantsverdriet, J. Corker, V. Vidal, A. Theolier, J. Thivolle-Cazat, J.-M. Basset, C. Nozkaki, C. G. Lugmair, A. T. Bell, T. D. Tilley, D. Kolb, K. P. De Jong, J. W. Geus, *Science* **2003**, *299*, 1688.

(3) J. R. Bhamore, S. Jha, A. K. Mungara, R. K. Singhal, D. Sonkeshariya, S. K. Kailasa, *Biosens. Bioelectron.* **2016**, *80*, 243.

(4) X. Jia, J. Li, L. Han, J. Ren, X. Yang, E. Wang, *ACS Nano* **2012**, *6*, 3311.

(5) H. Miao, D. Zhong, Z. Zhou, X. Yang, *Nanoscale* **2015**, *7*, 19066.

(6) P. Maity, S. Yamazoe, and T. Tsukuda, *ACS Catal.* **2013**, *3*, 182.

(7) Y. Nagai, K. Dohmae, Y. F. Nishimura, H. Kato, H. Hirata, N. Takahashi, *Phys. Chem. Chem. Phys.* **2013**, *15*, 8461.

(8) S. Vukojević, O. Trapp, J.-D. Grunwaldt, C. Kiener, F. Schüth, *Angew. Chem. Int. Ed.* **2005**, *44*, 7978.

(9) Y. Zhu, Y. Zhu, X. Kong, X. Li, G. Ding, Y. W. Li, *ACS Catal.* **2014**, *4*, 3612.

(10) M. E. Sad, M. Neurock, E. Iglesia, *J. Am. Chem. Soc.* **2011**, *133*, 20384.

(11) B. Bridier, M. A. G. Hevia, N. López, J. Pérez-Ramírez, *J. Catal.* **2011**, *278*, 167.

(12) C. W. Li, J. Ciston, M. W. Kanan, *Nature* **2014**, *508*, 504.

(13) K. Salorinne, X. Chen, R. W. Troff, M. Nissinen, H. Häkkinen, *Nanoscale* **2012**, *4*, 4095.

(14) N. Vilar-Vidal, J. Rivas, M. A. López-Quintela, *Phys. Chem. Chem. Phys.* **2014**, *16*, 26427.

(15) W. Yu, M. D. Porosoff, J. G. Chen, *Chem. Rev.* **2012**, *112*, 5780.

(16) R. Ferrando, J. Jellinek, R. L. Johnston, *Chem. Rev.* **2008**, *108*, 845.

(17) K. Jug, B. Zimmermann, P. Calaminici, A. M. Köster, *J. Chem. Phys.* **2002**, *116*, 4497.

(18) P. Jaque, A. Toro-Labbé, *J. Chem. Phys.* **2002**, *117*, 3208.

(19) S. Li, M. M. G. Alemany, J. R. Chelikowsky, *J. Chem. Phys.* **2006**, *125*, 34311.

(20) G. Guzmán-Ramírez, F. Aguilera-Granja, J. Robles, *Eur. Phys. J. D* **2010**, *57*, 49.

(21) G. H. Guvelioglu, P. Ma, X. He, R. C. Forrey, H. Cheng, *Phys. Rev. Lett.* **2005**, *94*, 26103.

(22) G. H. Guvelioglu, P. Ma, X. He, R. C. Forrey, H. Cheng, *Phys. Rev. B* **2006**, *73*, 155436.

(23) A. Poater, M. Duran, P. Jaque, A. Toro-Labbé, M. Solà, *J. Phys. Chem. B* **2006**, *110*, 6526.

(24) L. Padilla-Campos, *J. Mol. Struct.(THEOCHEM)* **2007**, *815*, 63.

(25) E. Fernández, M. Boronat, A. Corma, *J. Phys. Chem. C* **2015**, *119*, 19832.

(26) J. Barabás, T. Höltzl, *J. Phys. Chem. A* **2016**, *120*, 8862.

(27) B. R. Cuenya, *Thin Solid Films* **2010**, *518*, 3127.

(28) B. R. Cuenya, F. Behafarid, *Surf. Sci. Rep.* **2015**, *70*, 135.

(29) L. R. Merte, M. Ahmadi, F. Behafarid, L. K. Ono, E. Lira, J. Matos, L. Li, J. C. Yang, B. R. Cuenya, *ACS Catal.* **2013**, *3*, 1460.

(30) R. Reske, H. Mistry, F. Behafarid, B. R. Cuenya, P. Strasser, *J. Am. Chem. Soc.* **2014**, *136*, 6978.

(31) Y. Xia, Y. Xiong, B. Lim, S. E. Skrabalak, *Angew. Chem. Int. Ed.* **2009**, *48*, 60.

(32) M. E. Tess, P. L. Hill, K. E. Torraca, M. E. Kerr, K. A. Abboud, L. McElwee-White, *Inorg. Chem.* **2000**, *39*, 3942.

(33) H. Bönnemann, R. Brinkmann, P. Britz, U. Endruschat, R. Mörtel, U. A. Paulus, G. J. Feldmeyer, T. J. Schmidt, H. A. Gasteiger, R. J. Behm, *J. New Mater. Electrochem. Syst.* **2000**, *3*, 199.

(34) M. Estrella, L. Barrio, G. Zhou, X. Wang, Q. Wang, W. Wen, J. C. Hanson, A. I. Frenkel, J. A. Rodriguez, *J. Phys. Chem. C* **2009**, *113*, 14411.

(35) J. Nerlov, I. Chorkendorff, *Catal. Lett.* **1998**, *54*, 171.

(36) J. Nerlov, I. Chorkendorff, *J. Catal.* **1999**, *181*, 271.

(37) J. Nerlov, I. Chorkendorff, *Appl. Catal. A Gen.* **2000**, *191*, 97.

(38) Y. Yang, M. G. White, P. Liu, *J. Phys. Chem. C* **2012**, *116*, 248.

(39) Y. Yang, J. Evans, J. A. Rodriguez, M. G. White, P. Liu, *Phys. Chem. Chem. Phys.* **2010**, *12*, 9909.

(40) N. Austin, B. Butina, G. Mpourmpakis, *Prog. Nat. Sci. Mater. Int.* **2016**, *26*, 487.

(41) P. A. Derosa, J. M. Seminario, P. B. Balbuena, *J. Phys. Chem. A* **2001**, *105*, 7917.

(42) S. L. Han, X. Xue, X. C. Nie, H. Zhai, F. Wang, Q. Sun, Y. Jia, S. F. Li, Z. X. Guo, *Phys. Lett. Sect. A Gen. At. Solid State Phys.* **2010**, *374*, 4324.

(43) P. E. Blöchl, *Phys. Rev. B* **1994**, *50*, 17953.

(44) G. Kresse, D. Joubert, *Phys. Rev. B* **1999**, *59*, 1758.

(45) J. P. Perdew, K. Burke, M. Ernzerhof, *Phys. Rev. Lett.* **1996**, *77*, 3865.

(46) A. Seidl, A. Görling, P. Vogl, J. A. Majewski, M. Levy, *Phys. Rev. B* **1996**, *53*, 3764.

(47) H. Iikura, T. Tsuneda, T. Yanai, K. Hirao, *J. Chem. Phys.* **2001**, *115*, 3540.

(48) M. Kamiya, T. Tsuneda, K. Hirao, *J. Chem. Phys.* **2002**, *117*, 6010.

(49) T. Tsuneda, R. K. Singh, A. Nakata, *J. Comput. Chem.* **2016**, *37*, 1451.

(50) T. Tsuneda, R. K.Singh, A. Nakata, *J. Comput. Chem.* **2017**, *38*, 2020.

(51) M. Kamiya, H. Sekino, T. Tsuneda, K. Hirao, *J. Chem. Phys.* **2005**, *122*, 234111.

(52) R. K. Singh, T. Tsuneda, *J. Comput. Chem.* **2013**, *34*, 379.

(53) T. Tsuneda, R. K. Singh, *J. Comput. Chem.* **2014**, *35*, 1093.

(54) T. Tsuneda, S. Maeda, Y. Harabuchi, R. K. Singh, *Computation* **2016**, *4*, 23.

(55) J. W. Song, T. Hirosawa, T. Tsuneda, K. Hirao, *J. Chem. Phys.* **2007**, *126*, 154105.

(56) M. Couty, M. B. Hall, *J. Comput. Chem.* **1996**, *17*, 1359.

(57) C. Lee, W. Yang, R. G. Parr, *Phys. Rev. B* **1988**, *37*, 785.

(58) A. D. Becke, *J. Chem. Phys.* **1993**, *98*, 1372.

(59) A. D. Becke, *Phys. Rev. A* **1988**, *38*, 3098.

(60) J. P. Perdew, Y. Wang, *Phys. Rev. B* **1992**, *45*, 13244.

(61) Y. Zhao, D. G. Truhlar, *Theor. Chem. Acc.* **2008**, *120*, 215.

(62) Gaussian 16, Revision A.03, M. J. Frisch, G. W. Trucks, H. B. Schlegel, G. E. Scuseria, M. A. Robb, J. R. Cheeseman, G. Scalmani, V. Barone, G. A. Petersson, H. Nakatsuji, X. Li, M. Caricato, A. V. Marenich, J. Bloino, B. G. Janesko, R. Gomperts, B. Mennucci, H. P. Hratchian, J. V. Ortiz, A. F. Izmaylov, J. L. Sonnenberg, D. Williams-Young, F. Ding, F. Lipparini, F. Egidi, J. Goings, B. Peng, A. Petrone, T. Henderson, D. Ranasinghe, V. G. Zakrzewski, J. Gao, N. Rega, G. Zheng, W. Liang, M. Hada, M. Ehara, K. Toyota, R. Fukuda, J. Hasegawa, M. Ishida, T. Nakajima, Y. Honda, O. Kitao, H. Nakai, T. Vreven, K. Throssell, J. A. Montgomery, Jr., J. E. Peralta, F. Ogliaro, M. J. Bearpark, J. J. Heyd, E. N. Brothers, K. N. Kudin, V. N. Staroverov, T. A. Keith, R. Kobayashi, J. Normand, K. Raghavachari, A. P. Rendell, J. C. Burant, S. S. Iyengar, J. Tomasi, M. Cossi, J. M. Millam, M. Klene, C. Adamo, R. Cammi, J. W. Ochterski, R. L. Martin, K. Morokuma, O. Farkas, J. B. Foresman, and D. J. Fox, Gaussian, Inc., Wallingford CT, **2016**.

(63) M. Ernzerhof, J. Perdew, *J. Chem. Phys.* **1998**, *109*, 3313.

(64) J. P. Perdew, K. Burke, Y. Wang, *Phys. Rev. B* **1996**, *54*, 16533.

(65) J. P. Perdew, Electronic Structure of Solids '91; Ziesche, P.; Eschrig, H., Eds.; Akademie Verlag: Berlin, **1991**.

(66) Z. Fu, G. W. Lemire, G. A. Bishea, M. D. Morse, *J. Chem. Phys.* **1989**, *90*, 3417.

(67) R. Pou-Amérigo, M. Merchán, I. Nebot-Gil, P. Å. Malmqvist, B. O. Roos, *J. Chem. Phys.* **1994**, *101*, 4893.

(68) L. Lin, P. Claes, P. Gruene, G. Meijer, A. Fielicke, M. T. Nguyen, P. Lievens, *ChemPhysChem* **2010**, *11*, 1932.

(69) A. E. Reed, L. A. Curtiss, F. Weinhold, *Chem. Rev.* **1988**, *88*, 899.

(70) J. F. Janak, *Phys. Rev. B* **1978**, *18*, 7165.

(71) W. Yang, Y. Zhang, P. Ayers, *Phys. Rev. Lett.* **2000**, *84*, 5172.

(72) M. B. Knickelbein, *Chem. Phys. Lett.* **1992**, *192*, 129.

(73) O. Ingólfsson, U. Busolt, K. Sugawara, *J. Chem. Phys.* **2000**, *112*, 4613.

(74) P. K. Chattaraj, U. Sarkar, D. R. Roy, *Chem. Rev.* **2006**, *106*, 2065.

(75) R. G. Parr, W.Yang, *Density Functional Theory of Atoms and Molecules*; Oxford University Press: Oxford, U.K., 1989.

(76) T. A. Koopmans, *Physica* **1933**, *1*, 104.

(77) S. Noorizadeh, *Chin. J. Chem.* **2007**, 25, 1439.

(78) S. Noorizadeh, *J. Phys. Org. Chem.* **2007**, 25, 514.

(79) P. K. Chattaraj, *Ind. J. Phys.* **2007**, *81*, 871.

Table of Contents (TOC) Image

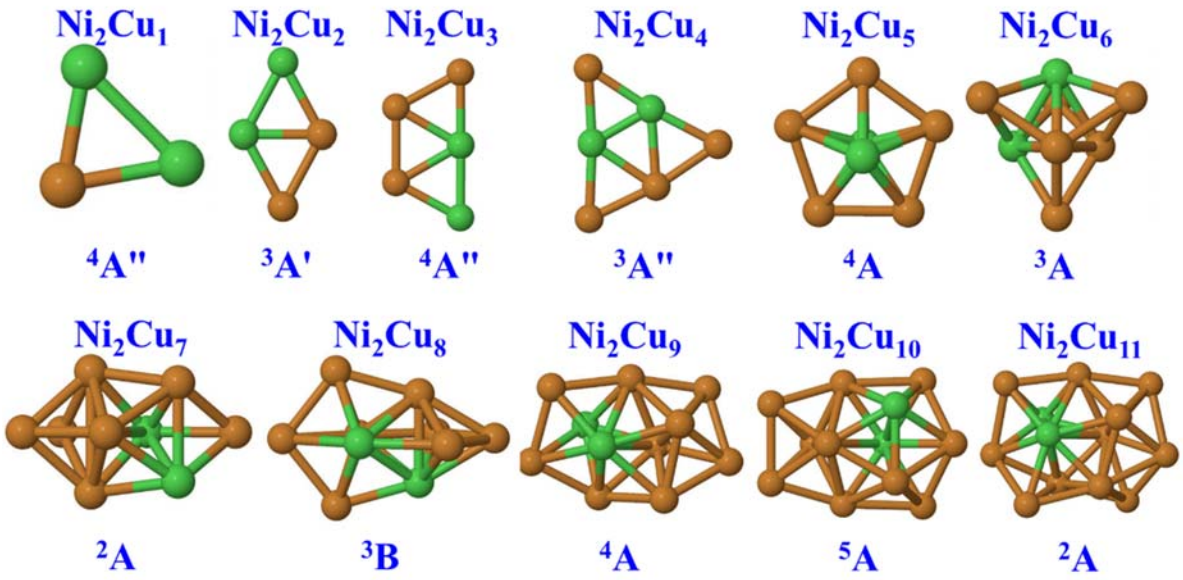

A systematic investigation of the lowest energy structures of Ni doped copper clusters are performed by doping one or two Ni atoms to the lowest energy structures of Cu_n with all possible atomic positions and possible spin multiplicities. In LC-DFT computations, the vertical ionization potentials calculated from HOMO energies give excellent agreement with the experimental values. It is shown that the substitution of Cu by Ni in the copper clusters enhances the chemical reactivity of large clusters.